Pure Appl. Chem., Vol. 84, No. 3, pp. 561–578, 2012.
http://dx.doi.org/10.1351/PAC-CON-11-07-10

Selective epoxidation of propylene to propylene oxide with H_2 and O_2 over Au/Ti-MWW catalysts*

Yingjie Ren, Le Xu, Liyan Zhang, Jianggan Wang, Yueming Liu, Mingyuan He, and Peng Wu‡

Shanghai Key Laboratory of Green Chemistry and Chemical Processes, Department of Chemistry, East China Normal University, North Zhongshan Rd. 3663, Shanghai 200062, China

Abstract: Direct epoxidation of propylene to propylene oxide (PO) with H_2 and O_2 has been performed on bifunctional catalysts, Au nanoparticles supported on novel Ti-MWW titanosilicate (Au/Ti-MWW). In comparison to conventional Au/TS-1 catalysts, Au/Ti-MWW exhibited a similar phenomenon with respect to PO formation, that is, the PO selectivity increased with increasing Si/Ti ratio of titanosilicate. However, at optimized Ti contents corresponding to Si/Ti ratio >140, the PO selectivity of Au/Ti-MWW catalysts was lower than 60 % in comparison to ca. 90 % achieved on Au/TS-1. A large number of boron species and defect-site-related hydroxyl groups contained in Ti-MWW were assumed to retard the desorption of PO from the channels or crystallite surface of zeolite, which favors side reactions such as over-oxidation and decomposition of PO. Poststructural rearrangement was then carried out on Ti-MWW with piperidine (PI) solution to improve effectively its hydrophobicity, leading to defect-less Re-Ti-MWW. This enhanced significantly the PO selectivity of Au/Re-Ti-MWW thus prepared, which reached as high as 92 % at Si/Ti ratio of 135. Au/Re-Ti-MWW(135) then gave the highest PO formation rate of 22.0 g_{PO} kg^{-1} h^{-1}.

Keywords: catalysis; epoxidation; gold nanoparticles; oxidation; propylene; propylene oxide; Ti-MWW; titanosilicate; zeolites.

INTRODUCTION

Propylene oxide (PO) is an important chemical intermediate that is widely used in the production of polyurethane, polyester resin, lubricants, surfactants, oil demulsifiers, and isopropanolamines. Several PO processes have been commercialized (Scheme 1). Conventional ones are mainly based on the chlorohydrin method using corrosive chlorine or co-oxidation techniques using expensive organic peroxides as oxidants (Scheme 1). PO production via chlorohydrin technology is a multistep process including the addition of hypochlorous acid to propylene to form chlorohydrin intermediates and subsequent dehydrochlorination of two chlorohydrin isomers to PO with calcium hydroxide. The chlorohydrin process then generates a stoichiometric amount of salt byproduct as well as a large quantity of halogen-containing waste water, which pose serious problems such as equipment corrosion, product separation, and environmental pollution. Additional capital costs are thus required, including more

Pure Appl. Chem.* **84, 411–860 (2012). A collection of invited papers for the IUPAC project 2008-016-1-300 "Chlorine-free Synthesis for Green Chemistry".

‡Corresponding author: Fax: +86-21 62232292; E-mail: pwu@chem.ecnu.edu.cn

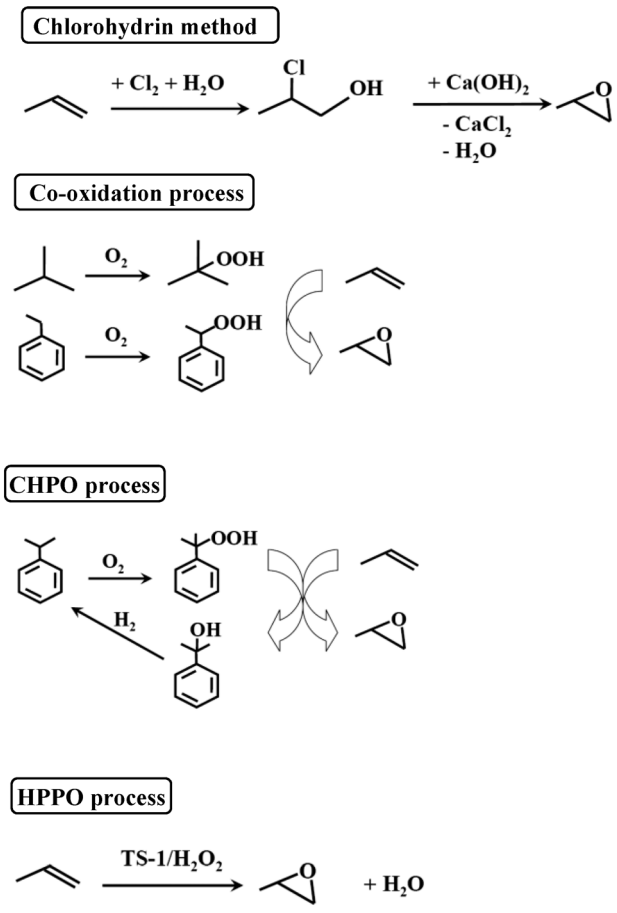

Scheme 1

extensive effluent treatment to handle the large dilute calcium chloride brine waste water. As the total chlorine losses are in the form of economically nonutilizable $CaCl_2$ or NaCl solutions, many efforts have been made to develop new oxidation systems based on chlorine-free methods.

Instead of the inorganic oxidant agent HOCl, organic oxide compounds have been selected to transfer the oxygen from the beginning to propylene [1]. Nevertheless, the co-oxidation processes using *tert*-butyl hydroperoxide and ethylbenzene hydroperoxide produce large quantities of coproducts such as *tert*-butanol and styrene in addition to PO. The whole process may suffer economic problems when the values of PO and coproducts become unbalanced. In a word, the above-mentioned PO processes coproduce a large amount of waste water together with organic and/or inorganic byproducts that need to be recycled or disposed of [2]. To avoid coproducing organic product, Sumitomo Chemical developed an innovative chlorohydrin PO process (CHPO) using cumene hydroperoxide as the oxidant, in which cumene is recycled via complicated and energy-consuming redox reactions.

The direct epoxidation of propylene to PO is a more preferable and simple alternative route in terms of greenness. Taking advantage of the unique catalytic properties of titanosilicates in liquid-phase selective reactions, BASF and Dow Chemical applied the TS-1/H_2O_2/methanol catalytic system (HPPO) to the PO process in 2008 [3,4]. Nevertheless, this innovative HPPO process needs to use expensive H_2O_2 as oxidant (Scheme 1). It also suffers some drawbacks, such as difficulty in separation owing to the azeotropic phenomena of methanol and PO, and moreover, the formation of solvolysis

byproducts of glycol ethers as a result of the ring-opening reaction of PO with methanol. A new direct PO process is thus expected to be developed.

In contrast to the commercial process of gas-phase epoxidation of ethylene with oxygen over a silver catalyst, the direct oxidation of propylene epoxidation with O_2 over Ag/Al_2O_3 catalyst usually gives a PO selectivity less than 50 % because the allylic hydrogen atoms in propylene are prone to be attacked by oxygen species to yield deep oxidation and/or combustion products [5–7]. The direct gas-phase epoxidation of propylene with H_2/O_2 mixture over supported Au catalysts has attracted many interests. Haruta and co-workers first reported in 1998 that Au/anatase catalysts prepared by deposition-precipitation (DP) method could catalyze the propylene epoxidation with H_2/O_2 at a PO selectivity >95 % at a low propylene conversion (~1 %) [8]. So far, considerable research has been carried out in this area, including the investigation of Au supported on titanosilicates [9–11]. The reaction is considered to be even greener and more energy-saving than the TS-1-based HPPO system. Delgass et al. found that a stable catalyst of 0.05 wt % Au/TS-1 (Si/Ti = 36) gave a propylene conversion of 8.8 % and a PO selectivity of 81 % at 473 K [12]. The same group also found that after NH_4NO_3 pretreatment, TS-1 could capture four times the amount of Au than an untreated sample, which remarkably enhanced the PO formation rate [10]. Another stable catalyst composition is Au supported on Ti-containing TUD mesoporous material on which the kinetics are shown to be similar to those on Au/TS-1 [13–15]. Haruta et al. reported that the Au nanoparticles deposited on a titanosilicate with wormlike mesopores show a propylene conversion of 8.5 % and PO selectivity of 91 % under optimized reaction conditions [9]. According to calculation, they concluded no substantial energy is needed when H_2 is co-fed with O_2 comparing with direct propylene expoxidation with O_2 alone [16]. It is believed that H_2 and O_2 react on Au nanoparticles to form H_2O_2, which then migrates to Ti sites to epoxidize propylene adsorbed there [13,14,17]. It is shown that the hydroperoxide species on the Ti site are the active species for epoxidation [18].

MWW-type titanosilicate (Ti-MWW) comprising two independent 10-membered ring (MR) channels and 12-MR cups on the crystal exterior, has been proven to be an efficient catalyst in liquid-phase epoxidation of various functional alkenes with H_2O_2 and ammoximation of ketones [19–21]. We have recently developed a method to enhance the hydrophobicity of Ti-MWW by post-rearrangement. Compared with directly synthesized Ti-MWW, the rearranged Ti-MWW shows an improved catalytic activity in the liquid-phase epoxidation and ammoximation reaction owing to enhanced hydrophobicity [21,22].

In this study, with the purpose to develop new catalysts for producing PO in a non-halogen system, we prepared Ti-MWW zeolites both by direct synthesis and post-rearrangement, and investigated the performance of Au catalysts supported on two types of Au/Ti-MWW by DP method in direct epoxidation of propene with H_2 and O_2.

EXPERIMENTAL

Preparation of Au/titanosilicate catalysts

Following the procedures reported previously [23], Ti-MWW supports were hydrothermally synthesized in the presence of boric acid using piperidine (PI) (MWW-type titanosilicate) as a structure-directing agent (SDA). Ti-MWW lamellar precursors were first synthesized at Si/Ti ratios of 30–240. The precursors were refluxed for 20 h in 2 M HNO_3 at a solid-to-liquid ratio of 1:50, which extracted the extra-framework titanium species together with a part of framework boron. For control experiments, TS-1 zeolites were synthesized at Si/Ti ratios of 35–240 according to the method patented by Enichem [24]. The samples were calcined in air at 823 K for 10 h to remove the organic species. With the purpose to enhance the hydrophobicity, the obtained Ti-MWW samples were structurally rearranged by post-modification in an aqueous solution of PI [22]. The treatment was carried out at PI/SiO_2 ratio of 1.0 and H_2O/SiO_2 ratio of 10 at 443 K for 1 day. The resulting solid was washed with deionized water, filtered,

dried at 373 K overnight, and finally calcined at 823 K for 6 h. The sample gained was denoted as Re-Ti-MWW.

Au/titanosilicate catalysts were prepared using the DP method. A 100-mL solution of $HAuCl_4 \cdot 4H_2O$ (1 g L^{-1}) was heated to 343 K under vigorous stirring. After the solution was neutralized with 0.5 M NaOH solution to reach the pH value of 7, 1 g of titanosilicate was added to form a suspension. After being stirred at 343 K for 1 h, the suspension was then cooled to ambient temperature. The solids were collected through filtration, washed with deionized water, and vacuum dried at room temperature overnight. The resulting products without further calcination are denoted as Au/Ti-MWW(*n*) or Au/TS-1(*n*) catalysts, where *n* represents the Si/Ti ratio.

Characterization methods

X-ray powder diffraction (XRD) patterns were measured on a Rigaku Ultima IV X-ray diffratometer with Cu-Kα radiation (λ = 1.5405 Å). UV–vis spectra were recorded on a Shimadzu UV-2400PC spectrophotometer with $BaSO_4$ as a reference. IR spectra were collected at room temperature on a NEXUS 670 spectrometer at a spectral resolution of 2 cm^{-1} after the self-supported wafer (30 mg, 20 mm Ø) was outgassed at 723 K for 3 h. ^{29}Si MAS NMR spectra were obtained on a Bruker DMX-500 spectrometer with a frequency of 79.43 MHz, a spinning rate of 3.0 kHz, and a recycling delay of 60 s. The chemical shift was referred to as Q_8M_8 $\{[(CH_3)_3SiO]_8SiO_{12}\}$. TEM images were taken on a JEOL-JEM-2100 microscope. Actual Au and Ti contents in the catalysts were determined by inductively coupled plasma (ICP) measurements on a Thermo IRIS Intrepid II XSP atomic emission spectrometer. The thermogravimetric and differential thermal analyses (TG-DTA) were performed on a METTLER TOLEDO TGA/SDTA851^e apparatus from room temperature to 1073 K at a heating rate of 10 K min^{-1} in air.

Catalytic testing

The epoxidation of propylene with H_2 and O_2 was carried out in a fixed-bed flow microreactor at atmospheric pressure, and the temperature was controlled with an electronic furnace. The catalyst powder (0.3 g) loaded in a quartz reactor (Ø 10 mm) was heated in a reaction gas mixture ($C_3H_6/H_2/O_2/N_2$ = 1/1/1/7 with a total flow rate of 20 mL min^{-1}) from room temperature to 423 K at a heating rate of 1 K min^{-1}. The reaction products were analyzed using three online gas chromatographs (GCs). The organic products were analyzed on the GC equipped with an FFAP capillary column and a flame ionization detector (FID). The amount of CO was determined with the GC equipped with a 5A molecular sieve compact column and a thermal conductivity detector (TCD). Another GC equipped with a TDX-01 compact column and a TCD was employed to detect CO_2. The carbon balance was close to 100 %. The propylene conversion and PO selectivity were calculated as follows:

Propylene conversion = moles of (oxygenates + 1/3CO_2)/moles of propylene in feed.

PO selectivity = moles of PO/moles of (oxygenates + 1/3CO_2).

RESULTS AND DISCUSSION

Properties and catalytic performance of Au catalysts on parent Ti-MWW

Figure 1 shows the XRD patterns of Ti-MWW and TS-1 synthesized at various Ti contents. In as-synthesized form, Ti-MWW was characteristic of a lamellar structure by showing the layer stacking-related [001] and [002] diffractions in the 2θ region of 3–7º (Fig. 1A). Upon acid treatment and further calcination, an interlayer dehydroxylation took place, which made the [001] and [002] diffractions almost disappear, indicating that a 3D MWW structure was constructed. Both Ti-MWW and TS-1 sam-

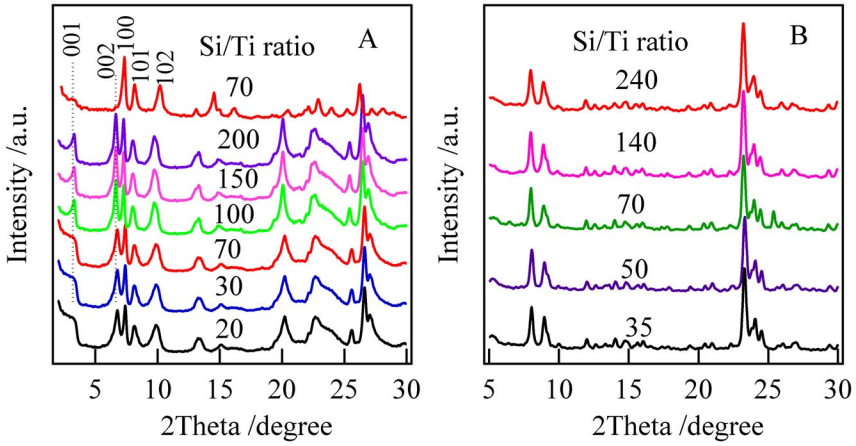

Fig. 1 XRD patterns of Ti-MWW (A) and TS-1 (B) as-synthesized at various Si/Ti ratios. The only exception shown on the top of left figure was taken on calcined Ti-MWW (Si/Ti = 70) for the sake of comparison.

ples showed the characteristic peaks of corresponding zeolite structures and had a high crystallinity without impurities of other phase-independent of Ti content.

Figure 2 shows representative UV–vis spectra of Ti-MWW(40) and TS-1(35), both with relatively high Ti content. The former was obtained corresponding lamellar precursor synthesized at Si/Ti = 20 by acid treatment. Both samples showed the main band at 210 nm, which is attributed to the isolated Ti species with a tetrahedral coordination [23]. No obvious band was observed around 330 nm, indicating the titanosilicates almost contained no anatase-like extra-framework Ti species. Thus, the samples were of good quality in terms of tetrahedrally coordinated Ti highly dispersed in the framework.

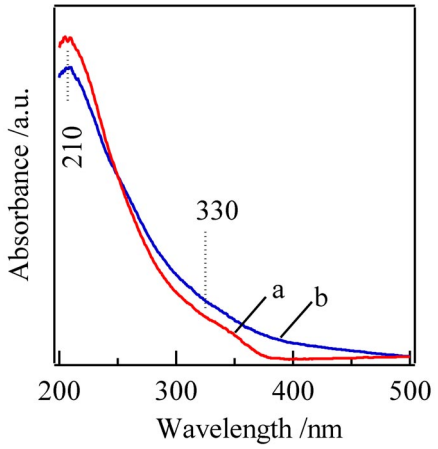

Fig. 2 UV–vis spectra of TS-1(35) (a) and Ti-MWW(40) (b). Ti-MWW(40) was obtained by acid refluxing the lamellar precursor synthesized at Si/Ti = 20 with 2 M HNO_3 at solid-to-liquid ratio of 1:50.

Au nanoparticles were then supported on Ti-MWW and TS-1 thus prepared by the DP method. Figure 3 shows the TEM images of two catalysts, Au/Ti-MWW(135) and Au/TS-1(140) together with that after spent in the gas-phase epoxidation of propylene with H_2 and O_2. The dark spots represented the supported Au particles. The Au particles observed on fresh Au/Ti-MWW(135) and Au/TS-1(140)

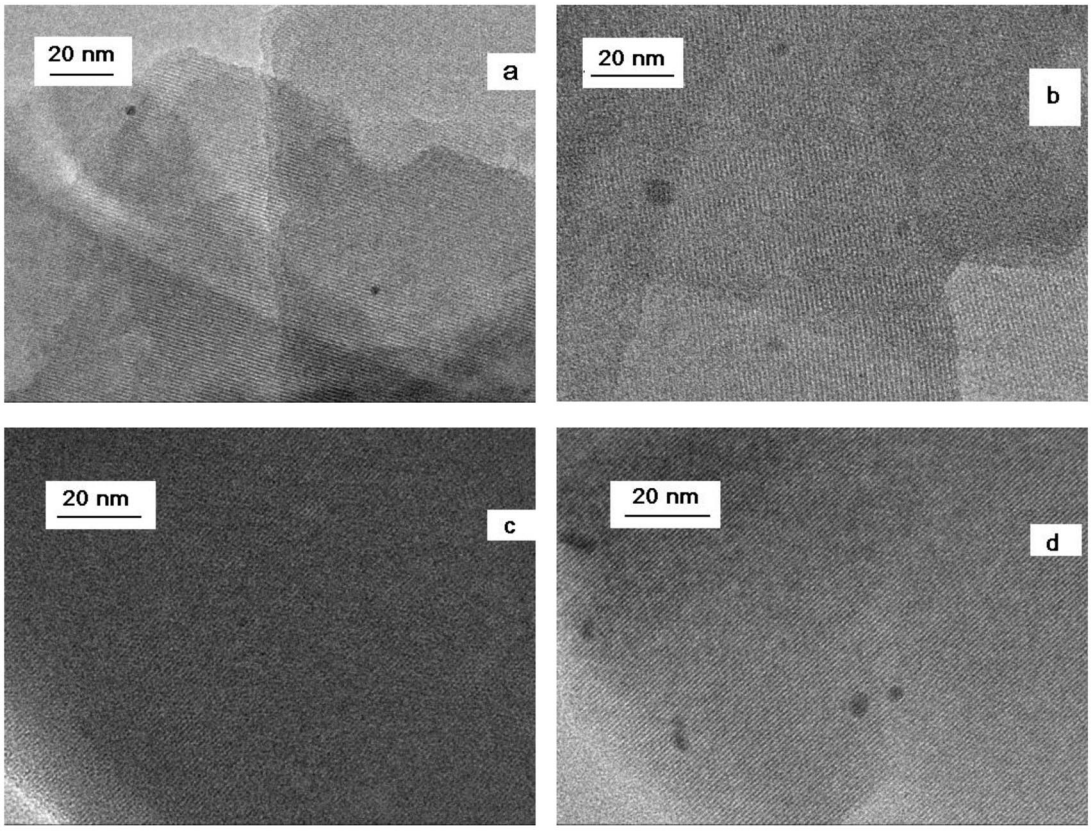

Fig. 3 TEM images of Au/Ti-MWW(135) (a,b) and Au/TS-1(140) (c,d) before reaction (a,c) or after spent in epoxidation of propylene with H_2 and O_2 at 423 K for 5 h.

had a size smaller than 5 nm (Figs. 3a,c). Only a handful of Au particles were visible in the selected area of TEM images, suggesting the Au particles were highly dispersed on the titanosilicate supports. Considering the fact that the pore entrance of TS-1 and Ti-MWW is only about 5.5 Å, the Au particles with nanoscale sizes were probably located on the outer surface of zeolite crystallites.

Table 1 summarizes the Au loading as well as catalytic results. Although the concentration of Au precursor used in DP solution was identical, the Au content actually supported on Ti-MWW or TS-1 changed with the Ti content. The Au loading increased slightly with increasing Ti content in Ti-MWW. A very similar variation was also observed for Au/TS-1. This is consistent with the results reported by other groups that higher Ti content leads to higher Au loading on TS-1 zeolite [12,25]. It seems that there is a certain affinity interaction between Ti species and Au precursor. The presence of Ti is helpful for capturing the Au precursor in the DP process. Moreover, compared at the same Si/Ti ratio, the Au content supported on Ti-MWW was higher than that on TS-1. This is probably related to more defect sites such as hydroxyl groups contained in Ti-MWW as shown below.

The Au/titanosilicate catalysts thus prepared were applied to the gas-phase epoxidation of propylene with H_2 and O_2 at 423 K. The reaction gave the products including CO, CO_2, H_2O, and C_3 compounds including PO, propane, propionaldehyde, acetone, and acrolein. The activities of catalysts were clearly related to the Au loading and Si/Ti ratio as shown in Table 1. Au/Ti-MWW(40) showed the highest initial conversion for propylene (5.1 %) among Au/Ti-MWW series, probably owing to its highest Au loading of 0.28 wt %. The initial activity was in the order of Au/Ti-MWW(40) > Au/Ti-MWW(70) > Au/Ti-MWW(135) > Au/Ti-MWW(165) > Au/Ti-MWW(225) > Au/Ti-MWW(350). The

Table 1 The results of propylene epoxidation over Au/Ti-MWW and Au/TS-1 with various Si/Ti ratios.[a]

Catalyst	Si/Ti ratio	Au (wt %)	C_3H_6 conv. (%)[a]	Product selectivity[b] (%)						PO formation rate (g kg^{-1} h^{-1})
				PO	Pn	PA	Ac	An	$CO+CO_2$	
Au/Ti-MWW(40)	40	0.28	5.1(1.5)	13.4(13.3)	13.0(15.9)	16.6(14.7)	13.1(8.7)	26.0(4.0)	16.0(39.5)	7.1(2.1)
Au/Ti-MWW(70)	70	0.24	3.1(2.0)	12.0(22.9)	10.8(13.0)	16.4(13.4)	7.1(6.2)	2.2(2.9)	46.9(39.5)	3.9(4.7)
Au/Ti-MWW(135)	135	0.19	2.5(2.1)	39.6(35.8)	9.3(11.6)	5.7(6.6)	5.3(6.7)	3.1(3.0)	37.0(36.2)	10.1(7.4)
Au/Ti-MWW(165)	165	0.16	1.5(1.4)	44.2(46.9)	12.0(12.7)	9.3(8.0)	5.7(4.9)	1.6(0)	27.2(27.6)	6.8(6.9)
Au/Ti-MWW(225)	225	0.13	1.5(1.4)	57.1(63.2)	12.1(11.2)	4.4(4.4)	3.9(3.3)	0(0)	22.6(17.8)	9.1(9.4)
Au/Ti-MWW(350)	350	0.1	1.4(1.3)	58.1(59.4)	13.7.6(9.0)	12.3(12.1)	7.8(9.7)	0(0)	8.2(9.8)	8.1(7.8)
Au/TS-1(35)	35	0.17	7.1(6.6)	33.7(37.2)	5.6(6.2)	8.4(8.8)	4.0(5.5)	1.3(1.6)	42.9(35.2)	24.8(25.3)
Au/TS-1(70)	70	0.12	4.6(2.1)	73.2(88.5)	5.2(0)	6.9(5.5)	2.9(0)	0(0)	11.9(6.0)	34.7(19.0)
Au/TS-1(140)	140	0.08	3.6(2.2)	89.0(88.0)	2.7(5.9)	2.3(2.0)	0(0)	0(0)	6.0(4.2)	32.8(20.0)
Au/TS-1(240)	240	0.05	3.1(2.4)	92.9(91.5)	0(0)	2.9(3.3)	0(0)	0(0)	4.2(5.2)	29.6(22.6)

[a]Reaction conditions: C_3H_6:H_2:O_2:N_2 = 1:1:1:7; space velocity = 4000 mL g^{-1} h^{-1}; T = 423 K. The data outside of and within parentheses were observed at TOS of 0.5 and 5 h, respectively.
[b]PO: propene oxide. Pn: propane. PA: propionaldehyde. Ac: acetone. An: acrolein.

lower the Si/Ti ratio, the lower the Au content and initial activity. The same phenomena were also observed on Au/TS-1 series, indicating Au/Ti-MWW catalyzed the epoxidation of propylene with H_2 and O_2 mixture with a similar mechanism as Au/TS-1. It is believed that H_2 and O_2 react on Au nanoparticles to form H_2O_2, which then migrates to the Ti sites to epoxidize propylene adsorbed [13,14,17]. Thus, it is comprehensible that more Au particles would promote in situ reaction of H_2 and O_2 to produce H_2O_2 and then favor the epoxidation of propylene on Ti sites.

The selectivity of PO was notably improved by increasing the Si/Ti ratios of Ti-MWW supports. The initial PO selectivity monotonically increased from 13.4 % on Au/Ti-MWW(40) to 58.1 % on Au/Ti-MWW(350) (Table 1). Meanwhile, the Au/TS-1 series showed a similar increasing trend when the Si/Ti ratio increased. However, not only showing a slightly higher propylene conversion, Au/TS-1 series catalyzed the epoxidation of propylene with a significantly higher selectivity to PO than that on Au/Ti-MWW (Fig. 4). With comparable Si/Ti ratios, Au/Ti-MWW(135) and Au/TS-1(140) showed the initial PO selectivities of 39.6 and 89.0 %, respectively. Even the highest PO selectivity observed on Au/Ti-MWW(350) was below 60 %, which was unsatisfied in comparison with Au/TS-1. Meanwhile, the deep oxidation products (mainly CO_2 together with CO) were produced at a higher level on Au/Ti-MWW than Au/TS-1.

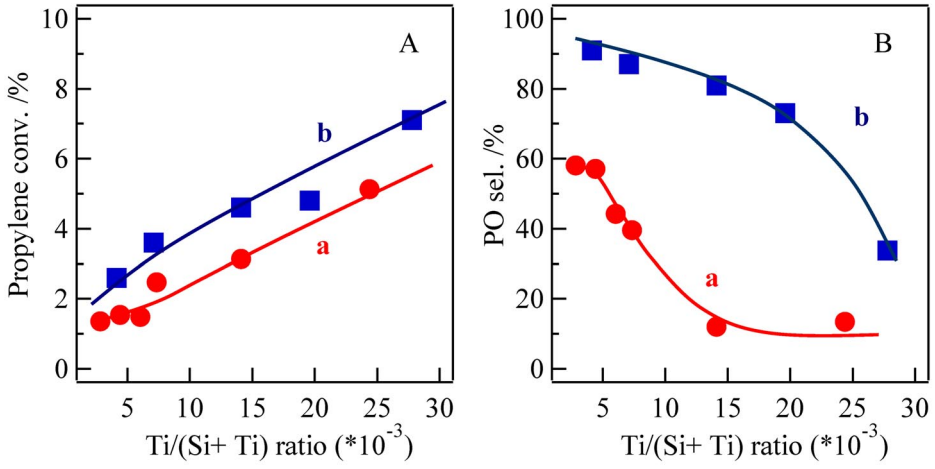

Fig. 4 Propylene conversion (A) and PO selectivity (B) as a function of Ti content in Au/Ti-MWW (a) and Au/TS-1 (b).

The stability is an important issue for propylene epoxidation over Au catalysts. In the present work, the steady state seemed to be reached after reaction for 5 h where the activity dropped more slowly than at the initial stage. The conversion of propylene was lowered at time on stream (TOS) of 5 h as indicated by the data shown in Table 1, implying a slight deactivation occurred during reaction. After they were spent in the PO formation reaction, some Au particles of Au/Ti-MWW(135) enlarged to 8~9 nm in diameter, although the others were still 3~5 nm in diameter (Fig. 3c). This indicates that the Au particles aggregated to some extent. The deactivation is then considered a result of sintering of the Au particles. On the other hand, the spent catalyst of Au/TS-1(140) still had a mean diameter of 3~5 nm (Fig. 3d). Despite the highest initial activity of Au/Ti-MWW(40), the degree of activity reduction during reaction was as large as 70 %. The corresponding data were 35, 16, 7, 7, and 7 %, for Au/Ti-MWW(70), Au/Ti-MWW(135), Au/Ti-MWW(165), Au/Ti-MWW(225), and Au/Ti-MWW(350), respectively. Increasing the Si/Ti ratio improved the stability of Au/Ti-MWW catalysts.

Figure 5 compares the performance of Au/TS-1 and Au/Ti-MWW at similar Si/Ti ratios (135–140) for propylene conversion, PO selectivity, and PO formation rate as a function of reaction

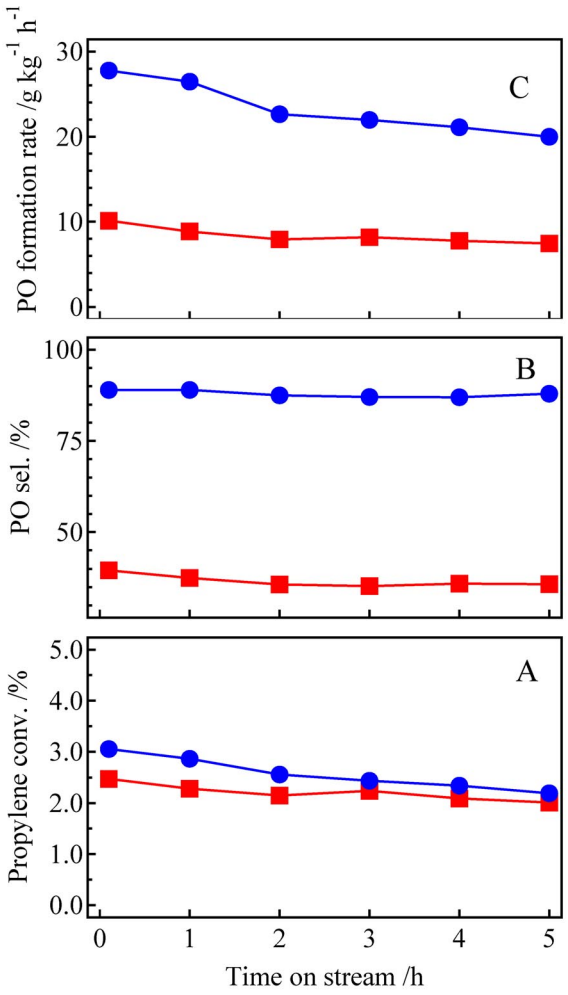

Fig. 5 Propylene conversion (A), PO selectivity (B), and PO formation rate (C) as a function of TOS for (■) Au/Ti-MWW(135) and (●) Au/TS-1(140). Reaction conditions, see Table 1.

time. Both the propylene conversion and PO selectivity of Au/Ti-MWW(135) were inferior to that of Au/TS-1(140). The difference in propylene conversion between two types of catalysts was not as significant as the gap in PO selectivity. As a combined result of propylene conversion and PO selectivity, the PO formation rate of Au/TS-1(140) was much higher than that of Au/Ti-MWW(135), which was obviously attributed to the difference in PO selectivity.

In addition to Au particles and Ti species, unsatisfied PO selectivity obtained with Au/Ti-MWW may be closely related to the structural difference between Ti-MWW and TS-1. Delgass et al. assumed that in gas-phase epoxidation of propylene, all partial oxidation products except acrolein went through PO first, while acrolein was produced from an unselective attack on the allylic hydrogen by oxygen [12]. They reported that the PO selectivity tended to decrease when the Au loading became high. It was assumed that the CO_2 yield was from either PO cracking on additional Au atoms or propylene combustion owing to the extra-framework Ti species existing in the supports. All samples used in this work showed in UV–vis spectra no adsorption at 330 nm associated with the extra-framework Ti species (Fig. 2), which suggests that the combustion of propylene is unlikely to happen. Thus, on

Au/Ti-MWW catalyst, the high selectivity to CO_2 and CO may be predominantly due to consecutive cracking of PO on the excess Au particles. The higher Au particle loading may also account for the poor stability of Au/Ti-MWW. Au aggregation is the main cause for deactivation of many supported Au catalysts [8,26–29]. It is generally accepted that only Au particles smaller than 5 nm are active and selective for epoxidation of propylene [8,26]. As shown in Fig. 3, the spent Au/Ti-MWW(135) catalyst possessed the Au particles with the size up to 8~9 nm. In the case of Au/TS-1(140), the Au particles remained smaller than 5 nm after reaction. These results indicate that the Au particles on Ti-MWW aggregated more easily than those on TS-1, leading to a rapid deactivation of the catalysts.

Moreover, the consecutive overoxidation of PO would take place more easily when it desorbs with difficulty from the channels and surface of the catalysts. That is to say, a rapid desorption of PO is critical to suppress the side reaction, and then contribute to a high PO selectivity. Generally, the acid sites and hydroxyl groups contained in titanosilicates may have a relatively strong interaction with the oxidation intermediates like PO, which retards its desorption. In addition to the silanol groups on the external surface and defect sites like hydroxyl nests, titanosilicates may contain another type of hydroxyl groups associated with the Ti species. Scheme 2 shows the local chemical environment around Ti sites in titanosilicates. The Ti tetrahedrally coordinated to four $[SiO]_4$ may exist as so-called "open" Ti sites as a result of hydration, resulting in the formation of Ti–OH and Si–OH groups [30]. Especially, the Si–OH groups adjacent to the Ti site exhibit a stronger acidity than weak acidic Si–OH groups on the external surface and/or internal vacancies. Thus, PO is preferably adsorbed firmly on the Si–OH sites adjacent to "open" Ti sites. This is the reason why when lowering the Ti content in titanosilicate, that is, reducing the amount of Si–OH groups on "open" Ti sites, the side reactions of PO were suppressed and the PO selectivity was improved obviously on both Au/Ti-MWW and Au/TS-1 catalysts (Fig. 4B). The PO desorption is also an important factor influencing the catalyst stability according to previous study on Au/TiO_2, $Au/TiO_2/SiO_2$, and Au/TS-1 catalysts [14,31]. Based on various characterizations, these researchers found that the strong adsorption of PO on adjacent Ti sites would form a bidentate species, leading to irreversible occupation of the active sites responsible for epoxidation. Our results were in agreement with previous reports. When the Ti content is decreased to a low level, e.g., Si/Ti > 100, the bidentate intermediate is less likely formed to deactivate the active sites.

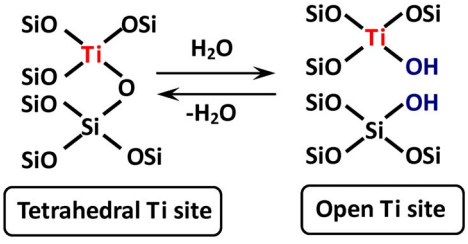

Scheme 2

However, since Ti-MWW was prepared from a B-containing system and derived from a lamellar precursor, it possessed more acid sites than TS-1 owing to abundant Si-OH groups on zeolite vacancies [23]. This is caused by acid washing and deboronation during preparation of Ti-MWW. Despite a weak acidity, the Si–OH groups on vacancies would also adsorb PO efficiently. Thus, the desorption of PO from Au/Ti-MWW was not as easy as from Au/TS-1 even at low Ti content, leading to a lower PO selectivity on Au/Ti-MWW. To enhance the PO selectivity of Au/Ti-MWW, it is necessary to improve its hydrophobicity. We once developed a poststructural rearrangement technique assisted by PI treatment that proved to be effective for reducing the amount of Si–OH groups in Ti-MWW [21,22].

Thus, Ti-MWW was first rearranged with PI and then supported with Au nanoparticles to investigate the catalytic performance in direct epoxidation of propylene to PO with H_2 and O_2.

Properties and catalytic performance of Au catalysts on rearranged Ti-MWW

The Ti-MWW samples with Si/Ti ratios from 70 to 225 were post-treated hydrothermally with PI solution and further calcined. The resultant products, denoted as Re-Ti-MWW, were characterized by various characterizations. UV–vis spectra of Re-Ti-MWW still showed a similar band predominantly at 210 nm (not shown), indicating the tetrahedral Ti sites remained intact in the framework.

Figure 6 shows the XRD patterns of the Ti-MWW samples with various Si/Ti ratios before and after the PI treatment as well as the graphic illustration for structural changes. The parent Ti-MWW samples had the 3D MWW structure with a closed interlayer pore entrance of 10-MR. In the framework, it contained the tetrahedral coordinated Ti and B atoms accompanied with a number of defect sites such as hydroxyl nests formed by deboronation and incomplete interlayer dehydroxylation (Fig. 6A). The post-treatment of parent 3D Ti-MWW with PI made the samples resort the [001] and [002] diffractions in the 2θ region of 3–7º, characteristic of a layered structure (Fig. 6B). During PI treatment, the interlayer spaces between Ti-MWW sheets were intercalated with PI molecules to reconstruct the lamellar structure. This type of structural interchange was almost independent of the Ti content. A further calcination at 803 K in air burned off the organic species occluded in the channels and posed a dehydroxylation between the layers. The 3D MWW structure was then reversibly reconstructed as the [001] and [002] diffractions owing to the layered structure disappeared (Fig. 6C). The XRD patterns of the calcined Re-Ti-MWW samples showed a negligible difference from those of parent ones in diffraction intensity, indicating a high crystallinity was maintained after these treatment sequences. As shown by the Si/Ti and Si/B ratio given by ICP, the PI treatment had no effect on the amount of Ti but deboronated slightly (Table 2). This is because the framework boron, having a relatively smaller ionic radius than the lattice silicon, is less stable in the silica matrix and tends to leach out of the crystalline structure under hydrothermal conditions. Thus, a reversible structural interchange between 3D MWW and lamellar precursor occurred during the hydrothermal treatment with PI solution and further calcination. The intercalation of PI molecules was the key guest molecule essential for an interlayer expanding [22]. The reversible structural change may induce a framework rearrangement, which made the framework Si species migrate into the neighboring hydroxyl nests or dehydroxylated partially the vicinal silanols to form the Si–O–Si linkage. This would mend the disconnection and increase the periodicity of the framework effectively. This kind of rearrangement has been realized often through so-called framework recrystallization by steaming in the case of aluminosilicates such as Y and mordenite zeolites [32,33], in which the dealumination vacancy can be removed to a certain degree. However, since the framework Ti species are more sensitive and delicate than the tetrahedral Al in terms of demetalation and change of the coordination state, the thermal and hydrothermal treatment is unsuitable for reducing the internal defect sites in the titanosilicates. Instead, the method of amine-assisted framework rearrangement has little influence on the Ti active sites but mends the MWW structure, leading to defect-less and more hydrophobic Ti-MWW zeolites.

Generally, the polar Si–OH groups may increase the hydrophilicity of titanosilicate [33,34]. Thus, the relative hydrophobicity of Re-Ti-MWW was measured through the procedures explored by Anderson and Klinowski [36]. The samples were calcined at 773 K to remove any adsorbed water. They were then hydrated at ambient temperature in a desiccator over a saturated NH_4Cl solution overnight. The amount of adsorbed water was then determined by thermogravimetry. The weight ratio of adsorbed water of Re-Ti-MWW to parent sample was 0.78–0.82. This indicated that the PI treatment increased the hydrophobicity, which is presumably due to partial removal of the hydroxyl groups at defect sites.

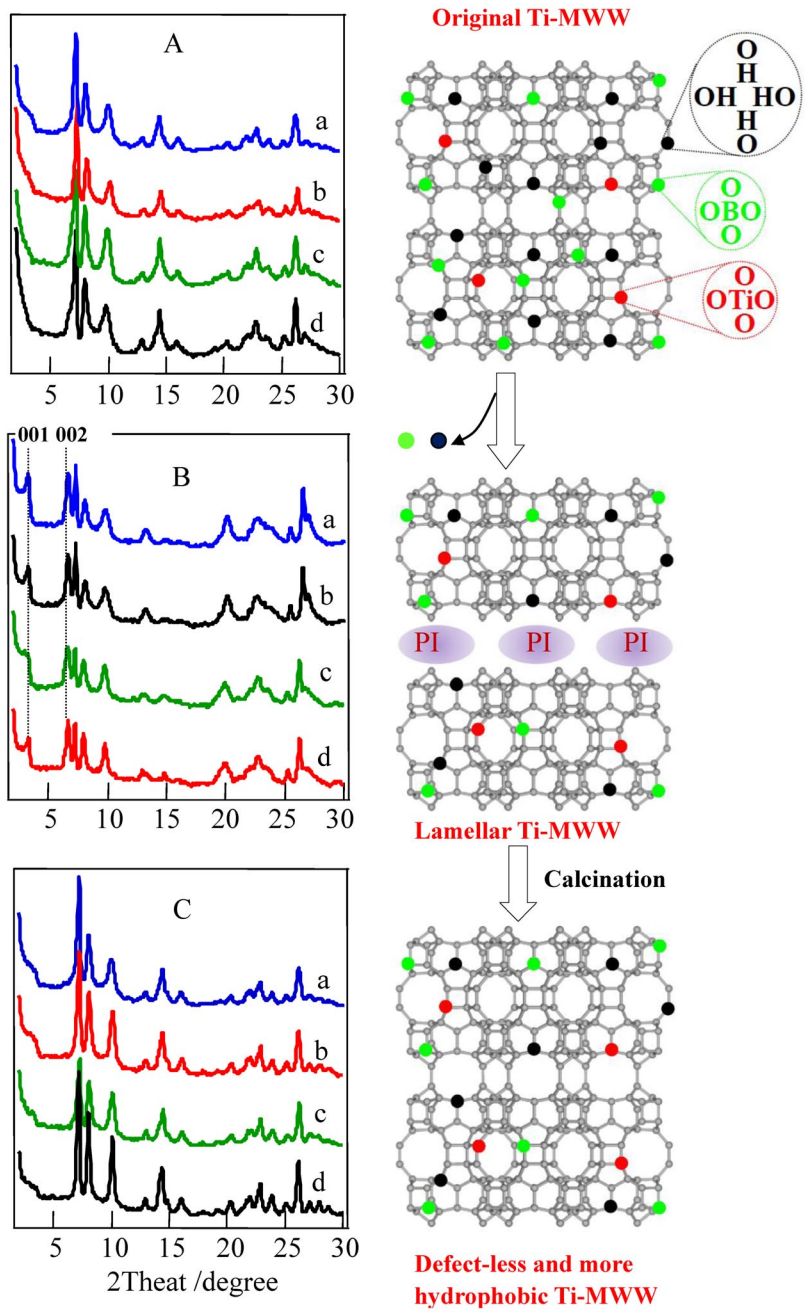

Fig. 6 XRD patterns of parent Ti-MWW (A), structurally rearranged Ti-MWW with PI treatment without (B) and with calcination (C). The Ti-MWW samples had a Si/Ti ratio of 40 (a), 135 (b), 165 (c), and 225 (d).

Table 2 Physicochemical properties of Ti-MWW before and after rearrangement.

No.	Before rearrangement			After rearrangement			Relative
	Si/Ti[a]	Si/B[a]	OH[c] (%)	Si/Ti[a]	Si/B[a]	OH[c] (%)	hydrophobicity[b]
1	70	42	–	70	53	–	0.82
2	135	41	100	135	51	65	0.81
3	165	49		165	62	–	0.80
4	225	46	100	225	57	63	0.78

[a]Given by ICP.

[b]Expressed in the ratio of water adsorbed after rearrangement to the parent sample. The amount of water adsorbed was determined by TG technique.

[c]The relative amount of OH groups was determined from the OH stretching vibration bands in IR spectra (3900–3000 cm^{-1}). The parent sample was assumed to contain 100 % OH groups.

In fact, both IR and NMR investigations verified that the hydroxyl groups in Ti-MWW decreased obviously following PI treatment. IR spectra in the hydroxyl stretching vibration were shown in Fig. 7. The parent Ti-MWW(135), Re-Ti-MWW(135), and TS-1(140) were taken as examples for comparison. The parent Ti-MWW(135) samples showed the band at 3745 cm^{-1} assigned to external or terminal silanols on the crystal surface, the band at 3725 cm^{-1} attributed to asymmetric hydrogen-bonded silanols located inside the crystals, and the band around 3550 cm^{-1} due to hydrogen-bonded silanol nests [37]. The internal silanols of Ti-MWW should originate from the defect sites as a result of deboronation and incomplete interlayer dehydroxylation during the preparation process. After the PI treatment, the OH stretching vibrations, particularly the bands at 3720 and 3500 cm^{-1}, decreased clearly in intensity. After the PI treatment, the hydroxyl groups were decreased by ca. 35 % (Table 2), estimating from the band area integrated in the region of 3000–3800 cm^{-1}. However, the amount of hydroxyl groups of Re-Ti-MWW(135) was still higher than that of TS-1(140).

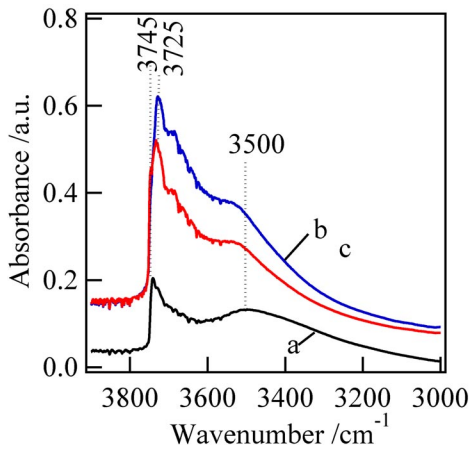

Fig. 7 IR spectra in hydroxyl stretching region of TS-1(140) (a), Ti-MWW(135) (b), and Re-Ti-MWW (135) (c) prepared after structural rearrangement with PI treatment at 443 K for 1 day and after calcination.

The removal of silanols by the structural rearrangement was further investigated by ^{29}Si MAS NMR spectroscopy (Fig. 8). It has been reported that MWW-type materials have at least eight crystallographically nonequivalent T sites [38], which has been supported by ^{29}Si MAS NMR spectroscopy [39]. The Q^4 sites in the region of –105 to –130 ppm could be assigned to several distinctive crystallographic sites in Ti-MWW but with overlapping resonances. The parent Ti-MWW

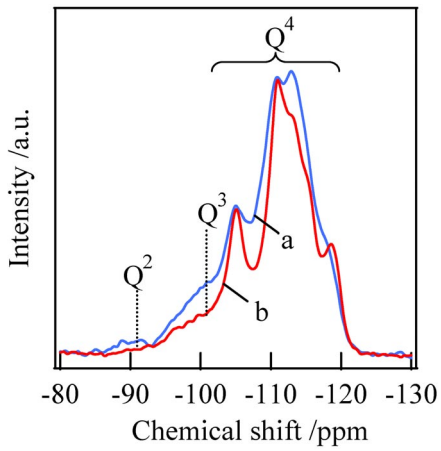

Fig. 8 ^{29}Si MAS NMR spectra of Ti-MWW(135) before (a) and after structural rearrangement with PI at 443 K for 1 day and calcination (b).

showed an obvious resonance at –103 ppm attributed to the Q^3 site, $Si(OH)(OSi)_3$ or $Si(OH)(OTi)(OSi)_2$. Compared with the unrearranged sample, Re-Ti-MWW showed similar resonances owing to the Q^4 sites but a less intensive Q^3 resonance at –103 ppm. This verifies that a portion of the defect sites disappeared definitely in the PI treatment. The quantitative data of the spectra simulation showed that the Q^3 sites were decreased by ca. 40 %, which was consistent with the above results evaluated with IR spectra.

The Au particles were also deposited on Re-Ti-MWW with the DP method and employed to the direct epoxidation of propylene. As summarized in Table 3, the Au loading on Re-Ti-MWW was a little lower than that on parent Ti-MWW shown in Table 1. A significant change following PI treatment was that the PO selectivity was greatly improved. Figure 9 shows the changes of propylene conversion, PO selectivity, and PO formation rate of Au/Re-Ti-MWW as a function of reaction time. Except for Au/Re-Ti-MWW(225), all the catalysts deactivated slowly with the reaction time and approached a steady state after 5 h. The PO conversion decreased with increasing Si/Ti ratio, while the selectivity to PO varied contrarily (Figs. 9A,B). It should be noted that all Au/Re-Ti-MWW catalysts showed a significantly enhanced selectivity to PO both at initial stage and steady state in comparison to corresponding Au/Ti-MWW with the same Si/Ti ratio. For Au/Re-Ti-MWW(70), Au/Re-Ti-MWW(135), and Au/Re-Ti-MWW(165), the activity was slightly lower than corresponding Au/Ti-MWW catalysts. Nevertheless, because of remarkably increased PO selectivity, the PO formation rate was improved on Au/Re-Ti-MWW catalysts (Fig. 9C). This is clearly related to the reduction of Si–OH groups in defect sites by post-treatment of Ti-MWW with PI and further calcination. The reduction of Si–OH groups would fasten the desorption of PO from zeolite surface and channels. This would minimize the consecutive side reactions and improve the selectivity to the objective product of PO. In the case of Au/Re-Ti-MWW(225), a low activity of 0.5 % may be due to too small Au loading of 0.09 wt %. The low Ti content and low Au loading could minimize the probability of Au adjacent to Ti sites. Thus, according to proposed reaction mechanism, H_2O_2 in situ produced on Au catalysts of Au/Re-Ti-MWW(225) could not effectively transfer to the distant Ti sites where epoxidation of propylene happened, leading to poor activity and a decreased PO formation rate.

Table 3 The results of propylene epoxidation over Au/Re-Ti-MWW[a].

Catalyst	Au (wt %)	C_3H_6 conv. (%)	Product selectivity[b] (%)						PO formation rate (g kg^{-1} h^{-1})
			PO	Pn	PA	Ac	An	$CO+CO_2$	
Au/Re-Ti-MWW(70)	0.24	2.7(1.7)	69.5(83.6)	5.5(0)	7.5(5.6)	3.3(2.4)	1.6(0)	12.6(8.4)	19.3(15.1)
Au/Re-Ti-MWW(135)	0.16	2.6(1.5)	81.9(91.9)	0(0)	5.7(3.2)	2.7(0)	1.2(0)	8.6(5.2)	22.0(14.2)
Au/Re-Ti-MWW(165)	0.13	1.5(0.9)	86.3(94.4)	0(0)	5.0(3.2)	2.7(0)	0(0)	6.0(2.5)	13.2(8.4)
Au/Re-Ti-MWW(225)	0.09	0.3(0.4)	86.9(94.0)	0(0)	0(6.0)	0(0)	0(0)	0(0)	3.1(3.5)

[a]Reaction conditions: see Table 1. The data outside of and within parentheses were observed at TOS of 0.5 and 5 h, respectively.
[b]PO: propylene oxide; Pn: propane; PA: propionaldehyde; Ac: acetone; An: acrolein.

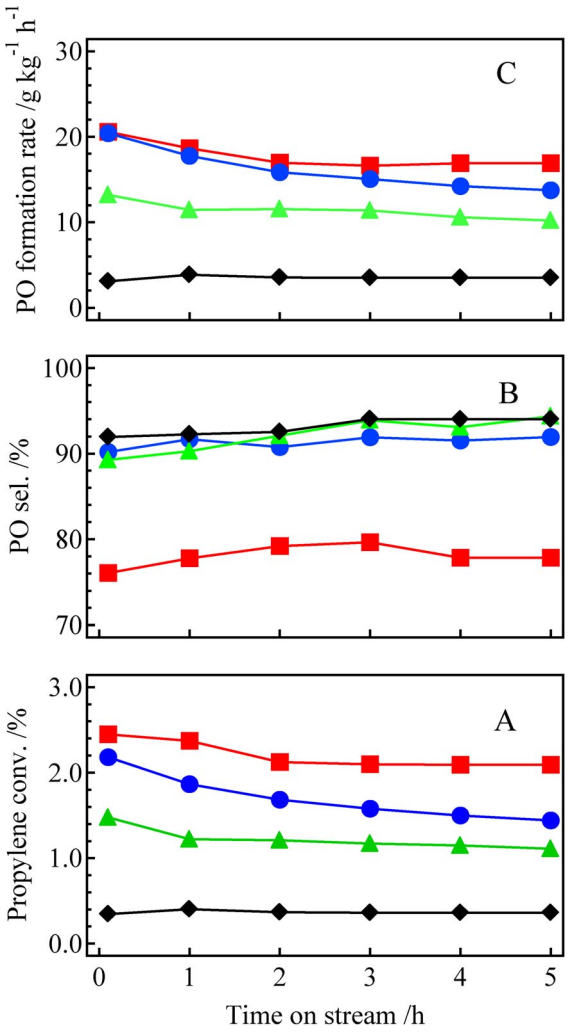

Fig. 9 Propylene conversion (A), PO selectivity (B), and PO formation rate (C) as a function of reaction time for (■) Au/Re-Ti-MWW(70), (●) Au/Re-Ti-MWW(135), (▲) Au/Re-Ti-MWW(165), and (◆) Au/Re-Ti-MWW(225).

The highest initial PO formation rate among the series of Au/Re-Ti-MWW catalysts was obtained on Au/Re-Ti-MWW(135). The value of 22.0 g_{PO} kg^{-1} h^{-1} was about twice as high as that achieved on Au/Ti-MWW(135). However, it was still inferior to the performance of Au/TS-1(140), which showed a PO value formation rate of 32.8 g_{PO} g^{-1} h^{-1}. Similar to Au/Ti-MWW described in the previous section, the difference may fall into two points: Au aggregation during reaction and hydroxyl groups of titanosilicates. Figure 10 shows the TEM images of Au/Re-Ti-MWW(135) before and after reaction for 5 h. The fresh catalyst had the Au particles with diameters smaller than 5 nm (Fig. 10a), which enabled the activity of catalysts. After reaction for 5 h, part of the Au particles aggregated to 8–9 nm (Fig. 10b). Comparing to the Au particles on Au/Ti-MWW(135), the aggregation of Au particles on the surface of structurally rearranged Re-Ti-MWW still took place. As shown in Fig. 7, although the hydroxyl groups were reduced partially by PI treatment and further calcination, Re-Ti-MWW(135) still showed stronger stretching bands than TS-1(140). These relatively abundant hydroxyl groups may be one of the factors influencing the activity of Au/Re-Ti-MWW(135). Nevertheless, these hydroxyl groups seemed to show no negative effects on selective formation of PO since the PO selectivity at steady state reached selectivity 91.9 % on Au/Re-Ti-MWW(135), which was even higher than that obtained on Au/TS-1(140) (88.0 %). Figure 11 shows the dependence of propylene conversion and PO selectivity

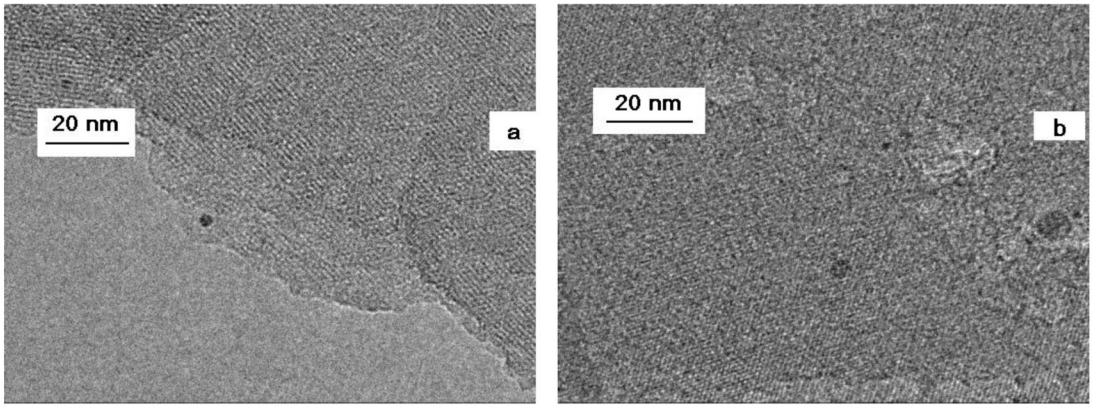

Fig. 10 TEM images of as-synthesized Au/Re-Ti-MWW(135) (a) and spent Au/Re-Ti-MWW(135) (b).

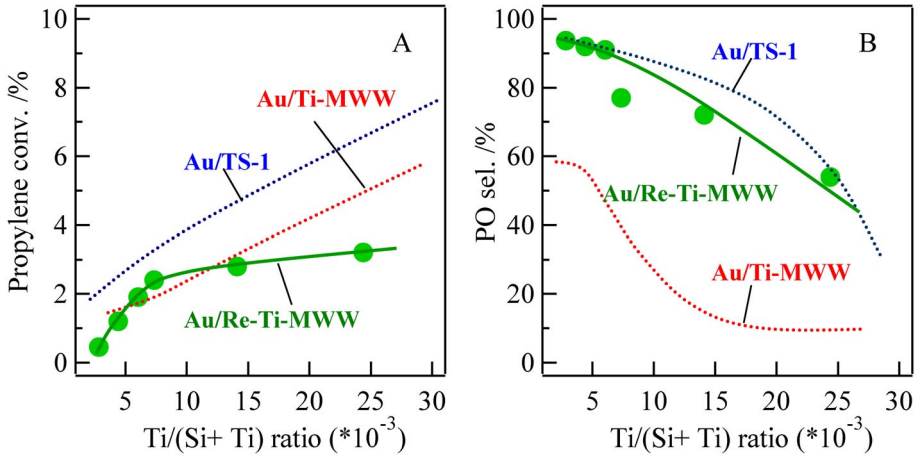

Fig. 11 Propylene conversion (A) and PO selectivity (B) as a function of Ti content in Au/Re-Ti-MWW. For comparison, the results of Au/Ti-MWW and Au/TS-1 are shown in dashed lines.

on the Ti content in various titanosilicates. Obviously, the structural rearrangement enhanced greatly the PO selectivity of Au/Ti-MWW.

In summary, we have prepared a new bifunctional catalyst for selective epoxidation of propylene with H_2 and O_2 via supporting Au nanoparticles on MWW-type titanosilicate. As shown in Scheme 3, the Au nanoparticles serve as the catalytic sites for in situ formation of H_2O_2 from H_2 and O_2 molecules. The H_2O_2 molecules then diffuse to the Ti sites located within the zeolite pores to induce the epoxidation of propylene to PO. To achieve a high PO selectivity, it is essential to shorten the residence time of PO within the pores and/or on the surface of catalyst to avoid over-oxidation of PO to CO_2, since Ti-MWW contains a large quantity of hydroxyl groups showing relatively strong interaction with PO molecules. This problem can be partially resolved by improving the hydrophobicity through structural rearrangement. Ti-MWW is a promising catalyst for selective expoxidation of propylene to PO in the gas phase.

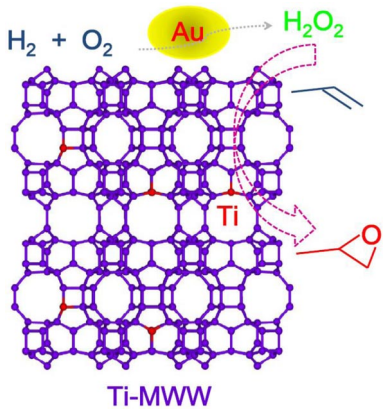

Scheme 3

CONCLUSIONS

Au catalysts supported on Ti-MWW are capable of catalyzing gas-phase epoxidation of propylene with H_2 and O_2. The activity decreases with increasing Si/Ti ratios while the PO selectivity varies contrarily. This is consistent with the trend observed on Au/TS-1, indicating that PO desorption from acid sites is important for suppressing side reactions and promoting PO production. Compared with Au/TS-1 catalysts, Au/Ti-MWW is less efficient in terms of PO selectivity, probably because of Au aggregation and the presence of abundant Si–OH groups. It is possible to enhance the hydrophobicity of Ti-MWW by structural rearrangement. The selectivity of PO is then significantly improved and reached 92 %, which is very comparable to the value achieved with TS-1 at the same Si/Ti ratio. Ti-MWW could be a good candidate for designing bifunctional catalyst suitable to the gas-phase epoxidation of propylene to PO.

ACKNOWLEDGMENTS

We gratefully acknowledge the National Natural Science Foundation of China (20890124, 20925310, 20873043), the Science and Technology Commission of Shanghai Municipality (09XD1401500), and the Shanghai Leading Academic Discipline Project (B409).

REFERENCES

1. K. Weissermel, H. J. Arpe. *Industrial Organic Chemistry*, Wiley-VCH, Weinheim (2003).
2. *Kirk-Othmer Encyclopedia of Chemical Technology*, 4th ed., Vol. 20, Watcher (Eds.), pp. 137–141, John Wiley, New York (1998).
3. A. Tullo. *Chem. Eng. News* **82**, 15 (2004).
4. A. R. J. H. Teles, P. Bassler, A. Wenzal, N. Rieber, P. Rudolf. U.S. Patent 67565032004 (2004).
5. M. Akimoto, K. Ichikawa, E. Echigoya. *J. Catal.* **76**, 333 (1982).
6. M. A. Barteau, R. J. Madix. *J. Am. Chem. Soc.* **105**, 344 (1983).
7. J. T. Roberts, R. J. Madix, W. W. Crew. *J. Catal.* **141**, 300 (1993).
8. T. Hayashi, K. Tanaka, M. Haruta. *J. Catal.* **178**, 566 (1998).
9. B. Chowdhury, J. J. Bravo-Suarez, M. Date, S. Tsubota, M. Haruta. *Angew. Chem., Int. Ed.* **45**, 412 (2006).
10. L. Cumaranatunge, W. N. Delgass. *J. Catal.* **232**, 38 (2005).
11. T. A. Nijhuis, T. Visser, B. M. Weckhuysen. *Angew. Chem., Int. Ed.* **44**, 1115 (2005).
12. B. Taylor, J. Lauterbach, W. N. Delgass. *Appl. Catal., A* **291**, 188 (2005).
13. J. Q. Lu, X. M. Zhang, J. J. Bravo-Suarez, K. K. Bando, T. Fujitani, S. T. Oyama. *J. Catal.* **250**, 350 (2007).
14. J. J. Bravo-Suarez, J. Lu, C. G. Dallos, T. Fujitani, S. T. Oyama. *J. Phys. Chem. C* **111**, 17427 (2007).
15. B. Taylor, J. Lauterbach, G. E. Blau, W. N. Delgass. *J. Catal.* **242**, 142 (2006).
16. J. H. Huang, T. Akita, J. Faye, T. Fujitani, T. Takei, M. Haruta. *Angew. Chem., Int. Ed.* **48**, 7862 (2009).
17. E. E. Stangland, B. Taylor, R. P. Andres, W. N. Delgass. *J. Phys. Chem. B* **109**, 2321 (2005).
18. J. J. Bravo-Suarez, K. K. Bando, J. I. Lu, M. Haruta, T. Fujitani, S. T. Oyama. *J. Phys. Chem. C* **112**, 1115 (2008).
19. P. Wu, T. Tatsumi. *J. Catal.* **214**, 317 (2003).
20. F. Song, Y. Liu, H. Wu, M. He, P. Wu, T. Tatsumi. *J. Catal.* **237**, 359 (2006).
21. L. Wang, Y. Liu, W. Xie, H. Zhang, H. Wu, Y. Jiang, M. He, P. Wu. *J. Catal.* **246**, 205 (2007).
22. L. Wang, Y. Liu, W. Xie, H. Wu, X. Li, M. He, P. Wu. *J. Phys. Chem. C* **112**, 6132 (2008).
23. P. Wu, T. Tatsumi, T. Komatsu, T. Yashima. *J. Phys. Chem. B* **105**, 2897 (2001).
24. T. Taramasso, G. Perego, B. Notari. U.S. Patent 44105011983 (1983).
25. J. Q. Lu, X. M. Zhang, J. J. Bravo-Suarez, T. Fujitani, S. T. Oyama. *Catal. Today* **147**, 186 (2009).
26. G. J. Hutchings. *Catal. Today* **100**, 55 (2005).
27. J. Schwank, S. Galvagno, G. Parravano. *J. Catal.* **63**, 415 (1980).
28. A. K. Sinha, S. Seelan, S. Tsubota, M. Haruta. *Angew. Chem., Int. Ed.* **43**, 1546 (2004).
29. A. K. Sinha, S. Seelan, M. Okumura, T. Akita, S. Tsubota, M. Haruta. *J. Phys. Chem. B* **109**, 3956 (2005).
30. Y. Wang, Y. Liu, X. Li, H. Wu, M. He, P. Wu. *J. Catal.* **266**, 258 (2009).
31. G. Mul, A. Zwijnenburg, B. van der Linden, M. Makkee, J. A. Moulijn. *J. Catal.* **201**, 128 (2001).
32. G. T. Kerr. *J. Phys. Chem.* **73**, 2780 (1969).
33. P. K. Maher, F. D. Hunter, J. Scherzer. In *Molecular Sieve Zeolites-I*, Vol. 101, E. M. Flanigen, L. B. Sand (Eds.), Chap. 21, pp. 266–278, American Chemical Society, Washington, DC (1974).
34. T. Tatsumi, K. A. Koyano, N. Igarashi. *Chem. Commun.* 325 (1998).
35. P. Wu, T. Tatsumi, T. Komatsu, T. Yashima. *Chem. Mater.* **14**, 1657 (2002).
36. M. W. Anderson, J. Klinowski. *J. Chem. Soc., Faraday Trans. 1* **82**, 1449 (1986).
37. G. P. Heitmann, G. Dahlhoff, W. F. Höderich. *J. Catal.* **186**, 12 (1999).
38. M. E. Leonowicz, J. A. Lawton, S. L. Lawton, M. K. Rubin. *Science* **264**, 1910 (1994).
39. G. J. Kennedy, S. L. Lawton, M. K. Rubin. *J. Am. Chem. Soc.* **116**, 11000 (1994).

